

Phonon drag thermoelectric phenomena in mesoscopic two-dimensional conductors: Current stripes, large Nernst effect, and influence of electron-electron interaction

O. E. Raichev ^{1,*}, G. M. Gusev ², F. G. G. Hernandez ², A. D. Levin,² and A. K. Bakarov ^{3,4}

¹*Institute of Semiconductor Physics, NAS of Ukraine, Prospekt Nauki 41, 03028 Kyiv, Ukraine*

²*Instituto de Física da Universidade de São Paulo, 135960-170, São Paulo, SP, Brazil*

³*Institute of Semiconductor Physics, Novosibirsk 630090, Russia*

⁴*Novosibirsk State University, Novosibirsk 630090, Russia*



(Received 15 July 2020; revised 20 October 2020; accepted 22 October 2020; published 6 November 2020)

The interaction of electrons with a flux of ballistic phonons leads to excitation of many angular harmonics of an electron distribution function. We show that this property dramatically modifies the magnetothermoelectric phenomena in two-dimensional electron systems with boundaries. By considering classical magnetotransport of electrons in a narrow channel with partly diffusive boundary scattering, we show that the phonon flux excites a pattern of current stripes with alternating directions of propagation along the channel. The Nernst voltage due to phonon drag appears already in the classical transport regime and can be comparable with the Seebeck voltage, while the latter acquires a dependence on the magnetic field. The temperature dependence of these voltages shows an unusual behavior determined by relaxation of higher-order harmonics of the distribution function via electron-electron scattering. Our experimental studies of mesoscopic samples based on high-quality GaAs quantum wells confirm the main properties of the thermoelectric response suggested by the theory.

DOI: [10.1103/PhysRevB.102.195301](https://doi.org/10.1103/PhysRevB.102.195301)

I. INTRODUCTION

The physics of thermoelectric phenomena in solids is an important field of study that has both fundamental and applied significance. In spite of a long research history, knowledge of the mechanisms of thermoelectricity is still not complete, and some experimental facts remain unexplained. In particular, one of the unsolved mysteries is an anomalously large Nernst effect due to phonon drag in two-dimensional (2D) electron systems in the classical transport regime [1,2]. The phonon drag mechanism implies that nonequilibrium acoustic phonons, having a net momentum along the temperature gradient ∇T , partly transfer this momentum to an electron system via their absorption and stimulated emission in the process of electron-phonon interaction, which resembles friction between electron and phonon subsystems. Indeed, in the regime of linear transport, this mechanism can be conveniently described [1,3] through a frictional force term, which is added to the Lorentz force term in the classical Boltzmann equation. If phonon distribution is established as a result of the linear response of a phonon system to a small temperature gradient, this distribution is weakly anisotropic [1,3,4], and the frictional force term is expressed through the “effective electric field” \mathbf{E}_ε^* proportional to ∇T . The typical conditions of thermoelectric experiments assume that the total current through the sample is zero. Thus, if the energy dependence of \mathbf{E}_ε^* is neglected, which is a good approximation for degenerate electron gas with energy ε replaced by the Fermi energy ε_F , the kinetic equation has a trivial solution describing the Seebeck field $\mathbf{E}_S = -\mathbf{E}^*$. In these conditions, the Nernst field \mathbf{E}_N (which is perpendicular

to both \mathbf{E}^* and magnetic field \mathbf{B}) is equal to zero since there is no current in the system. If the energy dependence of \mathbf{E}^* is taken into account, the effective electric field acts differently on electrons with different energies, and there appears a nonequilibrium distribution of electrons leading to a finite Nernst effect [5]. However, the corresponding Nernst field is proportional to a small factor $(T/\varepsilon_F)^2$, and it is much smaller than the Nernst field actually observed in experiments [6,7]. It was suggested [8] that the anisotropy of both the phonon and the electron spectra can be responsible for the large Nernst effect, but there is no direct proof of the relevance of this mechanism to the observed behavior. It is worth noting that the anomalously large Nernst effect due to phonon drag has been observed only in 2D systems, while in 3D systems this effect is negligibly small [9], in accordance with the theory. The properties described above correspond to the classical transport regime. In the quantum regime, i.e., when Landau quantization becomes important, the theory suggests a significant phonon-drag Nernst effect in 2D systems. Moreover, both Seebeck and Nernst coefficients show magnetophonon oscillations (see [10] and references therein).

Whereas the experiments described above have been done on macroscopic 2D samples, we have carried out measurements of Seebeck and Nernst voltages in small-sized (mesoscopic) bars, and we also observed an unexpectedly large classical Nernst effect, which we attribute to the phonon drag mechanism. In this paper, we propose a theory that relates the unusual classical phonon-drag Nernst effect to the presence of boundaries, and thus it can be helpful for the explanation of experimental results. We describe the behavior of magnetothermoelectric coefficients following from this theory, and we compare the results of calculations with our experimental data.

*Corresponding author: raichev@isp.kiev.ua

First of all, we notice that the phonon drag in small-sized 2D samples can occur due to the interaction of electrons with strongly nonequilibrium acoustic phonons coming directly from the heater, which creates a temperature gradient in the system. Indeed, at low temperatures, $T \sim 4.2$ K, the acoustic phonon mean free path lengths in crystals can be comparable to or even larger than the sample size, so the interaction of electrons with such ballistic phonons proves to be important [11–15]. While the interaction with quasiequilibrium phonons leads to a small momentum transfer to the electron system, of the order of drift momentum of a phonon per one collision, the electrons interacting with ballistic phonons gain much larger momenta, of the order of Fermi momentum. That is why the interaction of electrons with ballistic phonons often provides the main contribution to the drag, even if electron absorption of these phonons is relatively rare. Observation of large-amplitude magnetophonon oscillations of the drag-induced Seebeck voltages under conditions when T is much smaller than the Bloch-Grüneisen temperature also confirms the presence of strongly nonequilibrium high-energy (presumably ballistic) phonons in thermoelectric experiments [16,17].

The idea of our theory is based on the observation that the frictional force term describing the interaction of electrons with strongly nonequilibrium phonons is essentially different from the electric field term $e\mathbf{E} \cdot \mathbf{v}$ entering the linearized kinetic equation, and it cannot be represented through an effective electric field as described above. Whereas the electric field term depends on the cosine of the angle φ between the electric field \mathbf{E} and group velocity \mathbf{v} of an electron, i.e., it contains only the first angular harmonics ($\propto e^{\pm i\varphi}$), the frictional force term, in general, contains a set of different angular harmonics ($\propto e^{\pm ik\varphi}$). Thus, the interaction of electrons with a flux of ballistic phonons leads to excitation of many angular harmonics of electron distribution functions. In an ideal infinitely large and homogeneous 2D system, this important fact has no immediate significance, because only the first ($k = 1$) angular harmonics contributes to the current, and the condition of zero local current can be satisfied in the presence of electric field \mathbf{E} , which equilibrates the contribution from the first harmonics of the frictional force and describes the Seebeck effect ($\mathbf{E}_S = \mathbf{E}$) while the Nernst effect is absent ($\mathbf{E}_N = \mathbf{0}$). However, if the system is inhomogeneous, in particular when boundaries are present, there is a mixing of different angular harmonics of electron distribution, so the condition of zero local current cannot be satisfied. As a result, there should appear spatial distributions of electric current density and electrochemical potential, which depend on the system geometry and are sensitive to magnetic field. Such distributions are also sensitive to temperature T , mostly because an increase in T increases the probability of electron-electron scattering. This scattering is efficient in the relaxation of higher-order ($k \geq 2$) harmonics of the distribution function, and, for this reason, it is responsible for viscosity effects in electron systems, which have attracted a lot of attention [18] since the pioneering work of Gurzhi [19]. The current distribution implies the existence of both Seebeck and Nernst fields (and corresponding observable Seebeck and Nernst voltages), which are expected to have a nontrivial dependence on magnetic field and temperature.

To illustrate the basic properties of the transport regime described above and of its influence on magnetothermoelectric

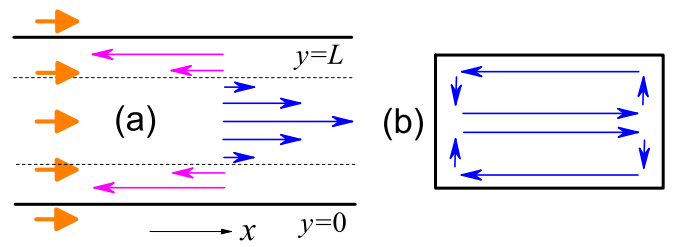


FIG. 1. Under excitation of electron system by a phonon flux (bold arrows) in a long channel, the electric current (thin arrows) flows in stripes with alternating directions so that the total current through the channel is zero (a). In finite-sized samples, such an excitation is expected to create current whirlpools (b).

phenomena, we consider 2D electrons confined in a straight channel ($0 < y < L$) in the presence of a transverse magnetic field B and a homogeneous unidirectional phonon flux, as shown in Fig. 1. We describe the results of the numerical solution of the classical Boltzmann equation with boundary conditions for partly diffusive boundary scattering. We find that in this geometry, the current density is arranged in a pattern of stripes with alternating directions of the current along the channel so that the total current is zero. If the boundaries are equivalent, the current distribution is symmetric and contains an odd number of stripes. At zero B , there are three or five such stripes, while with increasing B their number can increase. We calculate both the Seebeck field and Nernst voltage, and we find that a large Nernst effect can be expected. The Nernst voltage V_N is maximal for the case of fully specular boundary scattering. The Seebeck field does not depend on B in this specific case, but it becomes B -dependent for diffusive boundary scattering. In mesoscopic channels, whose width L is smaller than the mean free path length, the drag-induced Nernst voltage can be comparable with the Seebeck one, which is never the case in macroscopic samples. The increase of temperature leads to the suppression of the nonequilibrium spatial distribution of currents, as the electron-electron interaction suppresses the higher angular harmonics of the distribution function excited by the phonon flux, and internal friction within the electron gas tends to smoothen the current density distributions. As a result, the Nernst voltage decreases with increasing temperature. Our experimental data are in agreement with the main properties of thermoelectric response following from the theory.

The paper is organized as follows. Section II describes the theoretical model. The results of calculations are presented in Sec. III. Section IV contains a description of measurements and the experimental results, which are compared with the theoretical ones. More discussion and concluding remarks are given in the final section.

II. GENERAL FORMALISM

The distribution function of electrons moving in the electric field $\mathbf{E}(\mathbf{r}) = -\nabla\Phi(\mathbf{r})$ and the transverse magnetic field \mathbf{B} obeys the classical kinetic equation

$$\mathbf{v} \cdot \nabla f_{\mathbf{p}}(\mathbf{r}) + \left(e\mathbf{E}(\mathbf{r}) + \frac{e}{c}[\mathbf{v} \times \mathbf{B}] \right) \cdot \frac{\partial}{\partial \mathbf{p}} f_{\mathbf{p}}(\mathbf{r}) = \mathcal{J}_{\mathbf{p}}(\mathbf{r}), \quad (1)$$

where $\mathbf{r} = (x, y)$ is the 2D coordinate, $\mathbf{v} = \mathbf{p}/m$ is the group velocity, m is the effective mass, and \mathbf{p} is the 2D momentum of an electron. The right-hand side contains the collision integrals, including the one describing interaction of electrons with nonequilibrium phonons (Appendix A). Using energy and angle variables according to $\mathbf{p} = mv_\varepsilon(\cos \varphi, \sin \varphi)$, we write the distribution function as $f_{\mathbf{p}} \equiv f_{\varepsilon\varphi}$.

Below, we consider the geometry of infinitely long 2D channels of width L ($0 < y < L$, $-\infty < x < \infty$), and we assume a homogeneous (coordinate-independent) distribution of phonons. Under these conditions, the distribution function $f_{\varepsilon\varphi}$ does not depend on the x coordinate, the local currents along the y axis are absent, and the electrostatic potential is representable in the form $\Phi(\mathbf{r}) = -Ex + \Phi(y)$, where $E \equiv E_x$ is a homogeneous electric field. To solve the linear-response problem, it is convenient to write the distribution function as

$$f_{\varepsilon\varphi}(\mathbf{r}) = f_\varepsilon - \frac{\partial f_\varepsilon}{\partial \varepsilon} [g_{\varepsilon\varphi}(y) - e\Phi(y)], \quad (2)$$

where f_ε is the equilibrium Fermi distribution, and $g_{\varepsilon\varphi}$ describes a small nonequilibrium part of the distribution function. Substituting Eq. (2) into Eq. (1), one gets the following linearized kinetic equation for $g_{\varepsilon\varphi}$:

$$\left[\sin \varphi \frac{\partial}{\partial y} g_{\varepsilon\varphi}(y) + R_\varepsilon^{-1} \frac{\partial}{\partial \varphi} g_{\varepsilon\varphi}(y) - eE \cos \varphi - F_{\varepsilon\varphi} \right] \times \left(\frac{\partial f_\varepsilon}{\partial \varepsilon} \right) + \frac{\mathcal{J}_{\varepsilon\varphi}(y)}{v_\varepsilon} = 0, \quad (3)$$

where R_ε is the classical cyclotron radius for an electron with energy ε , and $\mathcal{J}_{\varepsilon\varphi}(y) = -(\partial f_\varepsilon / \partial \varepsilon) [J_{\varepsilon\varphi}^{\text{im}} + J_{\varepsilon\varphi}^{\text{ph}} + J_{\varepsilon\varphi}^{\text{ee}}]$ is the linearized collision integral describing interaction of electrons with impurities, equilibrium phonons, and other electrons. Next, $F_{\varepsilon\varphi}$ is the frictional force due to the phonon drag (see Appendix A). In the vicinity of the Fermi level (the case of degenerate electron gas is considered), we replace ε by the Fermi energy ε_F , v_ε by the Fermi velocity v_F , and we omit the energy index hereafter. The collision integrals are written in the relaxation-time approximation, with introduction of the characteristic mean free path lengths l_1 and l_e for momentum changing (electron-impurity and electron-phonon) and momentum conserving (electron-electron) scattering, respectively (see [20] and references therein). Then Eq. (3) is reduced to a partial differential equation

$$\left[\sin \varphi \frac{\partial}{\partial y} + R^{-1} \frac{\partial}{\partial \varphi} + \frac{1}{l} \right] g_\varphi(y) = \frac{g_0(y)}{l} + \frac{g_1(y) \cos \varphi}{l_e} + eE \cos \varphi + F_\varphi, \quad (4)$$

where $l = (1/l_1 + 1/l_e)^{-1}$, $g_0 = \int_0^{2\pi} d\varphi g_\varphi / 2\pi$, and $g_1 = \int_0^{2\pi} d\varphi \cos \varphi g_\varphi / \pi$.

The presence of the drag force F_φ makes Eq. (4) different from those considered earlier for the same geometry [20–23]. The boundary conditions for $g_\varphi(y)$ are [20]

$$g_\varphi(0) = r_\varphi^0 g_{2\pi-\varphi}(0) + (1 - r_\varphi^0) M_0, \quad (5)$$

$$g_{2\pi-\varphi}(L) = r_\varphi^L g_\varphi(L) + (1 - r_\varphi^L) M_L, \quad (6)$$

where $0 < \varphi < \pi$, the functions r_φ^0 and r_φ^L characterize reflection of electrons at the lower ($y = 0$) and upper ($y = L$) boundaries, while the constants M_0 and M_L are given by the following expressions: $M_0 = \mathcal{N}_0^{-1} \int_0^\pi d\varphi \sin \varphi (1 - r_\varphi^0) g_{2\pi-\varphi}(0)$, $M_L = \mathcal{N}_L^{-1} \int_0^\pi d\varphi \sin \varphi (1 - r_\varphi^L) g_\varphi(L)$, with $\mathcal{N}_{0,L} = \int_0^\pi d\varphi \sin \varphi (1 - r_\varphi^{0,L})$. Note that $r_\varphi^{0,L} = 1$ if $\varphi = 0$ or $\varphi = \pi$.

Application of the method of characteristics together with the boundary conditions allows one to obtain two coupled Fredholm equations ($n = 0, 1$) for the quantities $g_0(y)$ and $g_1(y)$:

$$g_n(y) = eE \mathcal{L}_n(y) + \Lambda_n(y) + \frac{1}{l} \int_0^L dy' \mathcal{K}_{n0}(y, y') g_0(y') + \frac{1}{l_e} \int_0^L dy' \mathcal{K}_{n1}(y, y') g_1(y'). \quad (7)$$

These quantities are related to local electrochemical potential (voltage) $V(y)$ and local current $j_x(y) \equiv j(y)$ according to $V(y) = g_0(y)/e$ and $j(y) = emv g_1(y)/2\pi \hbar^2$. The functions $\mathcal{L}_n(y)$, $\Lambda_n(y)$, and $\mathcal{K}_{nn'}(y, y')$ are specified in Appendix B. The terms $\Lambda_n(y)$ are determined by F_φ and are proportional to the intensity of phonon flux. Without these terms, Eq. (7) reduces to the one applied previously [20] to the problem of magnetoresistance of narrow channels. In the next section, we consider the case of equivalent boundaries, when $r_\varphi^0 = r_\varphi^L \equiv r_\varphi$, and we describe the thermoelectric response by applying the following expressions:

$$F_\varphi = eE_{\text{ph}} \text{sgn}(\cos \varphi), \quad (a)$$

$$F_\varphi = eE_{\text{ph}} \cos^2 \varphi \text{sgn}(\cos \varphi), \quad (b) \quad (8)$$

which correspond to interaction of electrons with either piezoelectric (a) or deformation (b) potential generated by unidirectional (along x) flux of acoustic phonons emitted by a black body whose temperature exceeds the Bloch-Grüneisen temperature (Appendix A). These expressions are referred to below as model [a] and model [b], respectively. If phonon flux is directed at an angle ϕ with respect to x , one should substitute $\varphi - \phi$ in place of φ in Eq. (8). If there is a symmetric deviation from unidirectional propagation, for example the phonons are propagating within an angular interval $-\delta < \varphi < \delta$ ($\delta < \pi/2$), then F_φ is modified, but the results presented below do not change qualitatively.

III. RESULTS

Consider first the case of zero magnetic field. In the absence of electron-electron interaction, $1/l_e \rightarrow 0$, there exists an analytical solution under condition $F_\varphi = F_{2\pi-\varphi}$, when phonon flux is directed along the channel or symmetrically distributed over the angles in an interval around $\varphi = 0$. For $0 < \varphi < \pi$,

$$g_\varphi = l(eE \cos \varphi + F_\varphi) \left[1 - \frac{(1 - r_\varphi) e^{-y/l \sin \varphi}}{1 - r_\varphi \lambda_\varphi} \right],$$

$$g_{2\pi-\varphi} = l(eE \cos \varphi + F_\varphi) \left[1 - \frac{(1 - r_\varphi) \lambda_\varphi e^{y/l \sin \varphi}}{1 - r_\varphi \lambda_\varphi} \right], \quad (9)$$

where $\lambda_\varphi = e^{-L/l \sin \varphi}$. The symmetry property $g_\varphi(y) = -g_{\pi-\varphi}(y)$ (since $F_\varphi = -F_{\pi-\varphi}$) leads to $M_0 = M_L = 0$, and $g_\varphi(y)$ satisfies the Fuchs-like boundary conditions [24,25] $g_\varphi(0) = r_\varphi g_{2\pi-\varphi}(0)$ and $g_{2\pi-\varphi}(L) = r_\varphi g_\varphi(L)$. The same symmetry makes $g_0(y)$ equal to zero. However, the local current $j(y) \propto \int_0^\pi d\varphi [g_\varphi(y) + g_{2\pi-\varphi}(y)] \cos \varphi$ is not zero. The requirement of zero total current $I = \int_0^L dy j(y) = 0$ defines the Seebeck field $E_S = E$ as

$$E_S = -\frac{I_F}{eI_E}, \quad \begin{pmatrix} I_F \\ I_E \end{pmatrix} = \int_0^\pi d\varphi \cos \varphi \begin{pmatrix} F_\varphi \\ \cos \varphi \end{pmatrix} \times \left[1 - \frac{l \sin \varphi (1 - r_\varphi)(1 - \lambda_\varphi)}{L (1 - r_\varphi \lambda_\varphi)} \right]. \quad (10)$$

If boundary reflection is specular, $r_\varphi = 1$, the factor in the square brackets is equal to 1. Then E_S is equal to its bulk value, $E_S = E_S^{\text{bulk}}$, which is determined by the first angular harmonics of F_φ :

$$E_S^{\text{bulk}} = -\frac{2}{e} \int_0^{2\pi} \frac{d\varphi}{2\pi} e^{\pm i\varphi} F_\varphi = -\frac{2}{e} \int_0^{2\pi} \frac{d\varphi}{2\pi} \cos \varphi F_\varphi. \quad (11)$$

In particular, $E_S^{\text{bulk}} = -(4/\pi)E_{\text{ph}}$ and $E_S^{\text{bulk}} = -(8/3\pi)E_{\text{ph}}$ for models [a] and [b], respectively. The solution $E_S = E_S^{\text{bulk}}$ for specular reflection is valid in the presence of electron-electron interaction and even in the presence of a magnetic field (see below). In the general case of partly diffusive boundary scattering, E_S depends on the ballisticsity ratio $b = l_1/L$ and on r_φ .

If electron-electron interaction is present, the local current density distribution is determined by the integral equation following from Eq. (7) at $n = 1$,

$$g_1(y) = l \int_0^\pi \frac{d\varphi}{\pi} \cos \varphi (eE \cos \varphi + F_\varphi) \times \left[2 - \frac{1 - r_\varphi}{1 - r_\varphi \lambda_\varphi} (e^{-y/l \sin \varphi} + e^{(y-L)/l \sin \varphi}) \right] + \frac{1}{l_e} \int_0^L dy' \mathcal{K}_{11}(y, y')|_{B=0} g_1(y'), \quad (12)$$

where $\mathcal{K}_{11}(y, y')$ at $B = 0$ can be obtained from Eq. (B1) as described in Appendix B. Without the phonon drag contribution F_φ , Eq. (12) coincides with the one from Ref. [26]. Once Eq. (12) is solved numerically, the Seebeck field $E_S = E$ is found from the relation of zero total current, $\int_0^L dy g_1(y) = 0$. The dependence of E_S on the ballisticsity ratio l_1/L for different ratios l_1/l_e is shown in Fig. 2. For wide channels, $l_1/L \rightarrow 0$, E_S is equal to its bulk value, while for narrow channels, E_S is smaller (model [a]) or larger (model [b]) than its bulk value because of the influence of boundaries. An increase of temperature T reduces the mean free path l_1 because of the contribution of electron-phonon scattering and increases the ratio l_1/l_e since l_e in a degenerate Fermi gas scales as T^{-2} , according to

$$l_e = A v_F \frac{\hbar \varepsilon_F}{T^2}, \quad (13)$$

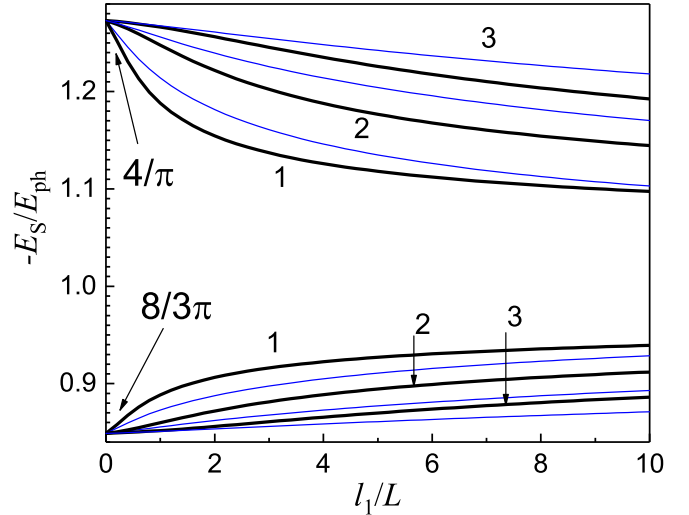


FIG. 2. Seebeck field in the absence of electron-electron scattering, $l_1/l_e = 0$ (1), and for finite electron-electron scattering, $l_1/l_e = 3$ (2) and $l_1/l_e = 10$ (3). The bold lines show the case of fully diffusive boundary scattering, $r_\varphi^0 = r_\varphi^L = 0$, while the thin (blue) lines correspond to weakly diffusive boundaries, $r_\varphi^0 = r_\varphi^L = \exp(-\alpha \sin^2 \varphi)$ with $\alpha = 1$. The upper and the lower groups of plots correspond to the models [a] and [b], respectively.

where A is a numerical constant. Therefore, with increasing T the absolute value of the Seebeck field approaches its bulk value by either increasing (model [a]) or decreasing (model [b]). This behavior is different from that expected in the commonly used model of weakly anisotropic phonon distribution [1,3], when the temperature dependence of the Seebeck field is determined by the factor $\ell_{\text{ph}}(\tau_{\text{ph}} T)^{-1}$, where ℓ_{ph} is the phonon mean free path with respect to phonon-phonon and phonon-impurity scattering, and τ_{ph}^{-1} is the rate of electron-phonon collisions. If electron gas is degenerate and T exceeds the Bloch-Grüneisen temperature, one has $\tau_{\text{ph}}^{-1} \propto T$, which means that the drag-induced Seebeck field in the weakly anisotropic phonon model should follow the temperature dependence of ℓ_{ph} and decrease with increasing T , which indeed is observed in GaAs-based 2D electron systems [27].

It is worth pointing out that the currents along the channel are absent, $j(y) = 0$ and $E = 0$, when phonon flux is perpendicular to the channel. The Seebeck voltage in this case develops along the y axis, $V_S = [g_0(L) - g_0(0)]/e$. The voltage distribution is determined by the integral equation $g_0(y) = \Lambda_0(y) + l^{-1} \int_0^L dy' \mathcal{K}_{00}(y, y')|_{B=0} g_0(y')$, where Λ_0 and \mathcal{K}_{00} at $B = 0$ can be found as described in Appendix B. If scattering is specular, $\Lambda_0(y)$ acquires a simple form $\Lambda_0(y) = l\pi^{-1} \int_0^\pi d\varphi F_\varphi [e^{(y-L)/l \sin \varphi} - e^{-y/l \sin \varphi}] / (1 + \lambda_\varphi)$. In the following, we do not consider this setup and always assume that phonon flux is parallel to the channel.

Consider now the case of nonzero magnetic field. For specular boundary scattering, $r_\varphi = 1$, the Seebeck field is a B -independent constant given by Eq. (11), $E_S = E_S^{\text{bulk}}$. To prove this equality, one may multiply Eq. (4) by $2 \cos \varphi$ and then integrate both of its sides over y from 0 to L and over φ from 0 to 2π . As a result, with the use of $I \propto \int_0^L dy g_1(y) = 0$,

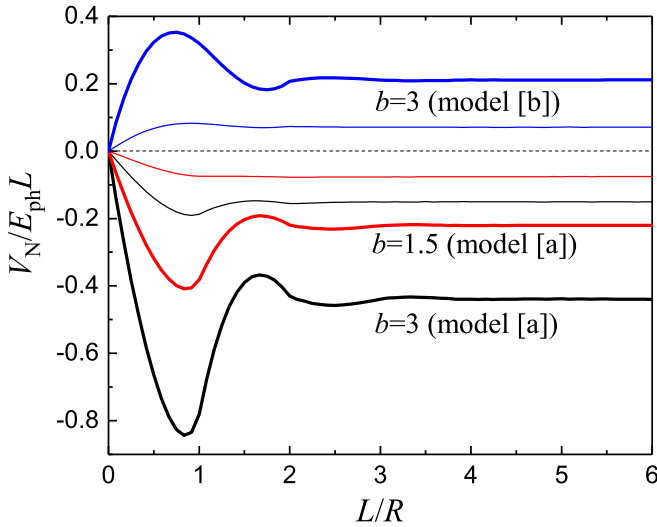


FIG. 3. Nernst voltage, as a function of magnetic field (expressed through $L/R \propto B$), in the case of specular boundary scattering for $l_1/L = 3$ and 1.5 , calculated for F_φ of Eq. (8). The bold lines are plotted assuming no electron-electron scattering, $l_1/l_e = 0$, and the thin lines show the case of finite electron-electron scattering, $l_1/l_e = 3$.

one obtains the identity

$$\int_0^{2\pi} \frac{d\varphi}{2\pi} \sin(2\varphi) [g_\varphi(L) - g_\varphi(0)] = L \left[eE + 2 \int_0^{2\pi} \frac{d\varphi}{2\pi} \cos \varphi F_\varphi \right]. \quad (14)$$

The boundary conditions for specular reflection are $g_\varphi(0) = g_{2\pi-\varphi}(0)$ and $g_\varphi(L) = g_{2\pi-\varphi}(L)$ so that $g_\varphi(L) - g_\varphi(0)$ is a symmetric function with respect to $\varphi = \pi$. Thus, the integral on the left-hand side of Eq. (14) is zero, and Eq. (14) is reduced to Eq. (10) with $r_\varphi = 1$. However, even for specular boundary reflection, $g_0(y)$ appears to be nonzero, because the homogeneous (y -independent) solution of Eq. (4) cannot satisfy the boundary conditions in the presence of magnetic field. Thus, a finite Nernst voltage $V_N = V(L) - V(0)$ develops. Figure 3 shows the dependence of V_N on B for different parameters $b = l_1/L$ and l_1/l_e . The sign of the Nernst effect is sensitive to the function F_φ describing excitation of the electron system and is different for the models [a] and [b]. Nevertheless, for both models the plots demonstrate a rapid increase of the absolute value of V_N in the low-field region, followed by a maximum. At larger magnetic fields, $L/R > 2$, the field dependence of V_N becomes very weak, so one can address saturation behavior. A full saturation, with a constant voltage $V_N = V_N^{\text{sat}}$, occurs at $L/R > 4$. The saturated Nernst voltage in the absence of electron-electron interaction is given by $V_N^{\text{sat}} = C_{\text{sat}} E_{\text{ph}} l_1$ with $C_{\text{sat}} = -0.148$ (model [a]) and $C_{\text{sat}} = 0.07$ (model [b]), so the effective Nernst field, defined as $E_N = V_N/L$, is proportional to the ballisticity ratio: $E_N^{\text{sat}} = C_{\text{sat}} E_{\text{ph}} b$. This means that in the samples of small size, where the ballisticity ratio is larger than unity, the Nernst and Seebeck fields in the classical transport regime can be comparable to each other. In macroscopic samples, however, the Nernst field is much smaller than the Seebeck one [6].

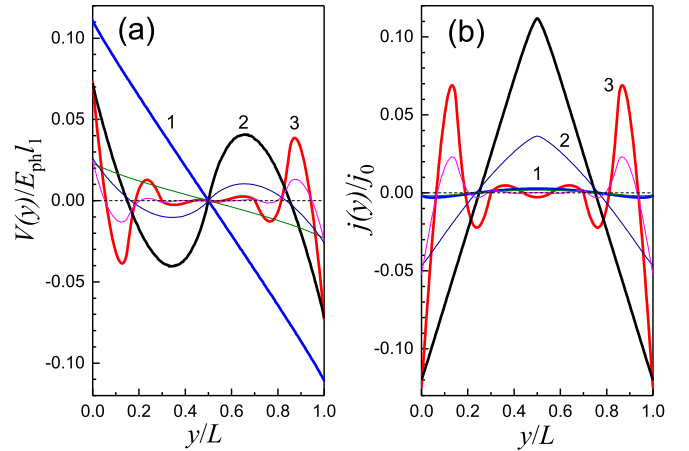


FIG. 4. Voltage (a) and current (b) distributions across the channel with specular boundary reflection for different magnetic fields: $R/L = 2$ (1), 0.5 (2), and 0.15 (3), calculated for F_φ of Eq. (8) (model [a]). There are nine current stripes at $R/L = 0.15$. The current density is expressed in units of $j_0 = \sigma E_{\text{ph}}$, where σ is the classical Drude conductivity at $B = 0$. The bold lines correspond to the absence of electron-electron scattering, $l_1/l_e = 0$, and the thin lines correspond to $l_1/l_e = 3$.

The electron-electron scattering leads to a decrease of the absolute value of V_N and makes the magnetic-field dependence of V_N smoother, in particular by suppressing its maximum. Indeed, the currents and electrochemical potentials (which are proportional to the first and zero angular harmonics of g_φ) appear in the channel because of the boundary-induced conversion of higher-order angular harmonics of g_φ excited by the phonon flux, whereas the electron-electron scattering suppresses these higher-order harmonics, thereby eliminating the source of the effect. If $l_1/l_e \rightarrow \infty$, V_N goes to zero. Although we have not succeeded in obtaining an analytical description of the saturated Nernst voltage, our analysis of numerical results suggests that, with a very high accuracy, it is approximated by $V_N^{\text{sat}} = E_{\text{ph}} l_1 C_{\text{sat}} / [1 + C_e l_1/l_e]$ with $C_e = 2/3$. Since the probability of electron-electron scattering is rapidly enhanced with temperature, the Nernst voltage is suppressed by temperature. In contrast, in macroscopic samples the phonon drag-induced Nernst voltage increases with temperature [5,6].

Figure 4 shows the distributions of local voltages and currents at different magnetic fields and demonstrates their suppression by the electron-electron scattering. At small magnetic fields, the currents are small and the voltage distribution is almost linear. As B increases, the voltage distribution becomes nonmonotonic. In stronger magnetic fields, when the cyclotron diameter $2R$ is smaller than $L/2$, there exists the region $2R < y < L - 2R$ where electrons do not feel the boundaries if moving ballistically, and where both the voltages and the currents become small. In this regime, the electrons near one boundary do not feel the other boundary, since an electron able to hit one of the boundaries cannot reach the other boundary even after a single scattering in the bulk, and the Nernst voltage loses its dependence on the channel width. The dependence on the magnetic field is lost as well, for the particular case of specular boundary scattering, which explains the saturation behavior shown in Fig. 3. When

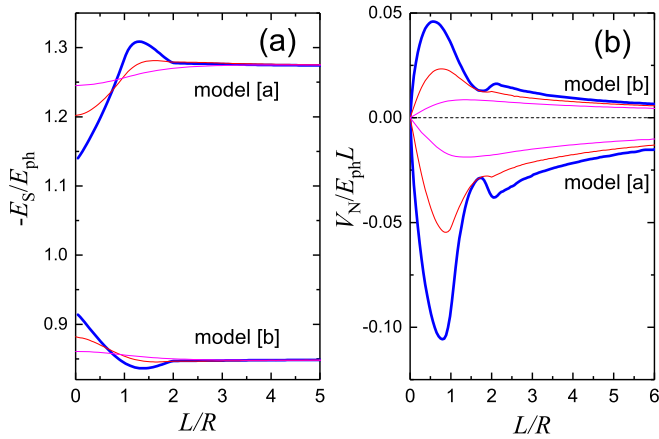


FIG. 5. Seebeck (a) and Nernst (b) voltages, as functions of the magnetic field (expressed through $L/R \propto B$), in the case of fully diffusive boundary scattering ($r_\varphi = 0$) for $l_1/L = 3$, calculated with F_φ of Eq. (8). The bold lines are plotted assuming no electron-electron scattering, $l_1/l_e = 0$, and the thin lines show the cases of finite electron-electron scattering, $l_1/l_e = 3$ (red) and $l_1/l_e = 10$ (magenta).

$R \ll L$, the current and voltage distributions near the boundary $y = 0$ are the same as in the semi-infinite plane $y > 0$.

For partly diffusive boundary scattering, $r_\varphi < 1$, the magnetic-field dependence of the Nernst voltage V_N does not show a well-defined saturation. Instead, V_N slowly decreases with B at $2R < L$. Also, V_N becomes gradually smaller when the diffusivity of the scattering increases, because the current appearing in the system is reduced by the boundary scattering. As a consequence, the temperature-induced suppression of V_N becomes weaker with decreasing r_φ . The dependence of V_N on B is weakly sensitive to the form of reflection coefficient r_φ . With regard to the Seebeck field E_S , the diffusivity of the boundary scattering leads to a qualitatively new feature, a dependence of E_S on B : the absolute value of E_S tends to reach the bulk value E_S^{bulk} at $L/R \gg 1$. Thus, in the case when $|E_S| < |E_S^{\text{bulk}}|$ at $B = 0$ (model [a]), $|E_S|$ increases with B , while in the opposite case (model [b]), $|E_S|$ decreases with B . An example of the B -dependence of V_N and E_S is shown in Fig. 5.

IV. EXPERIMENT AND THEORY

We have measured the thermoinduced voltages in the samples based on the high-quality GaAs quantum wells with electron density $n_s \simeq 6.6 \times 10^{11} \text{ cm}^{-2}$ and low-temperature mobility $\mu \simeq 2.1 \times 10^6 \text{ cm}^2/\text{Vs}$. We have studied mesoscopic-size H-shaped four-terminal bars consisting of a central channel of length $10 \mu\text{m}$ and width $L = 4 \mu\text{m}$ between symmetrically placed $5\text{-}\mu\text{m}$ -wide legs (see the inset in Fig. 6). The temperature gradient is directed along the channel. The details of the experimental setup and measurements are given in the Supplemental Material [28]. The Seebeck and the Nernst voltages were measured by a lock-in detector at a frequency of $2f_0 = 0.8\text{-}2.5 \text{ Hz}$. The thermoelectric measurements were performed in a variable temperature insert cryostat in the temperature range from 4.2 to 40 K in magnetic fields up to 0.5 T. Above 0.2 T, we observe magnetophonon oscillations

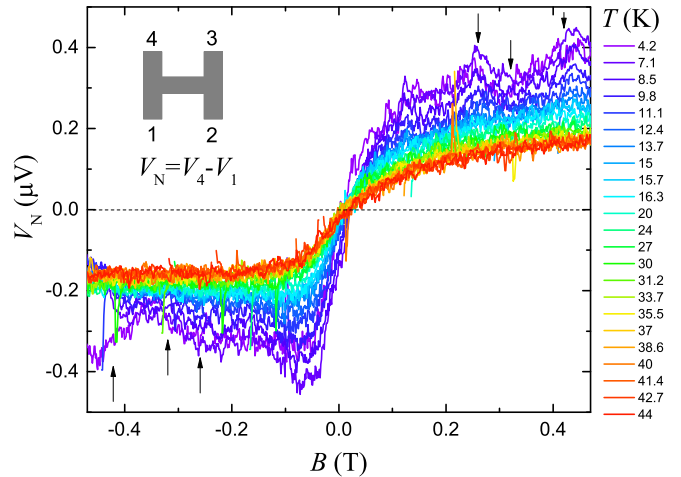


FIG. 6. Magnetic-field dependence of the Nernst voltage $V_N = V_{14}$ at different temperatures. The arrows indicate calculated positions of the maxima and minima of the magnetophonon oscillations.

both in the Seebeck and in the Nernst voltages, indicating the importance of the phonon drag mechanism.

Below we concentrate on the Nernst effect measurements, since the influence of magnetic field and temperature on the Seebeck effect expected from the theory is rather weak to be resolved experimentally, regarding the level of noise present in our measurements. The plot of the Nernst voltage in a wide region of magnetic fields and temperatures at a fixed heater power is shown in Fig. 6. The Nernst voltage rapidly increases with B in the region $B < 0.1 \text{ T}$, where the classical transport regime is expected, and it shows signs of saturation above 0.1 T. This voltage decreases considerably with increasing T in the whole range of the magnetic fields. In contrast, the Seebeck voltage (Fig. 7) does not show a significant temperature dependence. Such a behavior is different from that expected for the diffusion mechanism of thermoelectricity, which was studied earlier in mesoscopic systems [29–32]. This is expected, because in GaAs quantum wells the diffusion mechanism is much weaker than the phonon drag mechanism in the interval of temperatures that we study. However, the behavior of thermoinduced voltages we observe is also different from that caused by the phonon drag in macroscopic samples. The most striking feature is the magnitude of the Nernst voltage, V_N , which is comparable to the Seebeck voltage, V_S , measured at the same heater power, Fig. 7. Another unusual feature is a strong suppression of V_N when temperature T increases from 4.2 to 40 K. The transition from strong to weak (or saturated) $V_N(B)$ dependence takes place between 0.05 and 0.1 T, which correlates with the field $B = 0.068 \text{ T}$ corresponding to the condition $2R = L$ for this particular device. Therefore, taking also into account that the mean free path l_1 in our device is larger than L , one may attribute the observed unusual magnetothermoelectric behavior to the size effect. The increase in temperature, apart from the general suppression of the Nernst effect, causes a smoothing of the $V_N(B)$ dependence; in particular, it washes out the peak visible at small negative B .

The mechanism of magnetothermoelectric effects in mesoscopic samples proposed in the previous sections can explain the basic unusual features listed above. In Fig. 8, we have

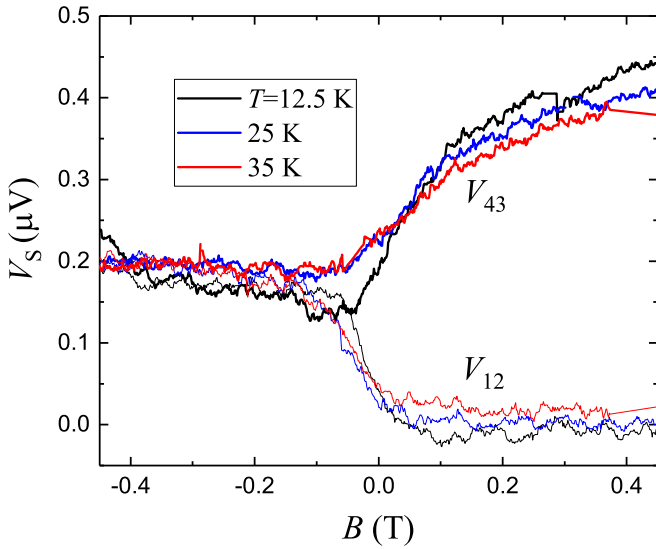


FIG. 7. Magnetic-field dependence of the Seebeck voltages measured between the upper and lower pairs of contacts for several temperatures (indicated). The heater driving voltage is 2 V, the same as in the Nernst effect measurements shown in Fig. 6.

plotted both the Seebeck field (which is related to the Seebeck voltage as $-E_S = V_S/L_x$, where L_x is the distance between the voltage probes along the channel) and the Nernst voltage V_N , calculated for a channel of width $L = 4 \mu\text{m}$. We have used the parameters of our sample such as the electron density and temperature dependence of the resistivity in the pristine 2D layer [28], which defines the temperature dependence of the mean free path length l_1 . The length l_e was estimated according to Eq. (13) with $A = 5$ determined from the temperature dependence of magnetoresistance in similar Hall bar mesoscopic devices [20]. To describe the boundary scattering, we use $r_\phi = \exp(-\alpha \sin^2 \phi)$ with $\alpha = 3$. The function F_ϕ has been taken from Eq. (A7) containing two terms. Parametrically, the first term in Eq. (A7) dominates in our samples, so the behavior of thermoelectric effects is characteristic for the model [b]. This behavior is consistent with the sign of the observed Nernst effect. In contrast to the Nernst effect, the evolution

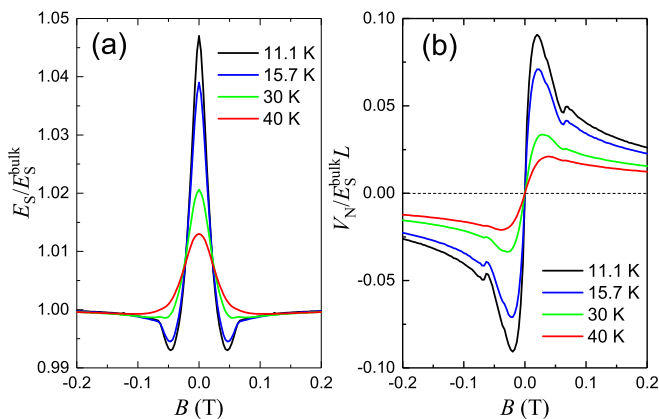


FIG. 8. Magnetic-field dependence of Seebeck field (a) and Nernst voltage (b) calculated for the channel of width $L = 4 \mu\text{m}$, based on the parameters of the device studied in the experiment, for several temperatures.

of the Seebeck voltage with magnetic field is expected to be small, never exceeding 5% of the total effect, suggesting that experimental discrimination between the models [a] and [b] is a difficult task for nanovolt scale measurements. In addition, in the region of weak magnetic fields, the Seebeck voltages measured at the upper (V_{43}) and at the lower (V_{12}) pairs of contacts are different and show a different dependence on the magnetic field; see Fig. 7 and [28]. We do not have an explanation of the asymmetry of V_{43} and V_{12} with respect to the sign of B and of their strong difference in the region of positive B . This may be related to contact imperfections, leading to asymmetry of the contact resistances, combined with contributions of skipping orbits to transport.

The calculations show that the absolute value of the Seebeck field decreases slightly with magnetic field, it has a weak local minimum at $B \sim 0.05 \text{ T}$, which is washed out by temperature T , and it saturates at the bulk value at $B > 0.1 \text{ T}$, where it becomes independent of T . The Nernst voltage V_N first increases with B , goes through a sharp maximum at $B \simeq 0.02 \text{ T}$, and slowly decreases at $B > 0.07 \text{ T}$, where $2R < L$. When T increases from 11 to 40 K, V_N at large B decreases approximately twice, which agrees with our experimental data (Fig. 6). The smoothing of the $V_N(B)$ dependence with increasing temperature is also in agreement with the experiment. According to the calculations, the observed temperature-induced suppression of the Nernst effect cannot be explained by a reduction of l_1 due to interaction of electrons with equilibrium phonons; this suppression occurs mostly because of the reduction of l_e , i.e., due to the increase of electron-electron scattering probability. In spite of the basic similarities between experimental and theoretical plots, there are differences between them. The experiment does not show a strong maximum of the Nernst voltage at $B \simeq 0.02 \text{ T}$. Instead, a weaker maximum is seen between 0.05 and 0.1 T and only in the region of negative B . The magnitude of the observed Nernst effect, as compared to the magnitude of the Seebeck effect, is considerably larger than that suggested by the theory. We do not expect, however, a direct correlation between theory and experiment because the theory uses a number of simplifying assumptions, in particular a simple device geometry and a model distribution of nonequilibrium phonons that dictates the form of F_ϕ . The actual distribution of phonons over their energies and angles is unknown, and most likely is different from the one used in the calculations. The geometry of our experiment is more complicated compared to the simple long channel geometry because the side arms 1–4 cannot be described merely as voltage probes; the distribution of currents and potentials in these arms is also important for developing the thermoelectric response. In particular, in addition to the horizontal current stripes in the central section, we expect vertical current stripes in the arms, and the overall current distribution may even include whirlpool patterns similar to those described in Ref. [33]. In magnetic field, the distributions of currents and potentials in the upper (4,3) and lower (1,2) side arms are expected to be different from each other. The presence of the arms increases the absolute value of the Nernst voltage compared to that in the simple long channel geometry, which is actually observed, because the effective vertical size (width) of the device becomes considerably larger. Next, the sharp features at $2R = L$

and the prominent peaks at smaller magnetic fields in the theoretical plots of V_N are a consequence of the single size scale, i.e., the channel width L , appearing in the theory. In the real device, there is no such single size scale, and this can explain the absence of both the prominent peaks and the sharp features in the observed magnetic-field dependence of the Nernst voltage. Nevertheless, the observed suppression of the Nernst voltage by temperature is expected to be weakly sensitive to either device geometry or phonon distribution, and our theory provides a reasonably good description of this unusual behavior.

V. SUMMARY

Earlier experimental studies of magnetothermoelectric phenomena in small-sized (mesoscopic) 2D electron systems were concentrated on the diffusive mechanism of thermoelectricity, as the temperature gradient in electron gas was created by heating of electrons by current, thereby avoiding nonequilibrium phonon fluxes across the samples [29–32]. In our work, we have used a more conventional experimental setup by placing a heater near the mesoscopic system, and we have obtained an unusual thermoelectric response attributed to the phonon drag mechanism, which is known to dominate over the diffusive mechanism in GaAs-based samples in the interval of temperatures we study [1,2]. To explain the observation of a large Nernst effect in the classical transport region, we have proposed a theoretical model based on the assumption that the phonon distribution function is considerably different from the weakly nonequilibrium distribution usually applied for a theoretical description of the phonon drag thermoelectricity. This is the case when the main contribution to the drag effect comes from the ballistic phonons arriving at the 2D layer directly from the heater, which is relevant even in macroscopic samples [17]. Interaction of electrons with such phonons leads to excitation not only of the first angular harmonics of the electron distribution function, but also of the higher-order harmonics. We have shown that in the presence of boundaries causing a mixing of different angular harmonics due to the diffusivity of boundary scattering or even due to specular boundary reflection in a magnetic field, the electron system undergoes a transition to a peculiar state characterized by a nonhomogeneous current pattern in the form of stripes with alternating directions of propagation, leading to a Nernst voltage that can be comparable to the Seebeck one. From this perspective, our basic experimental findings can be viewed as manifestations of the size effect in the thermoelectric properties. We note that there are other ways for excitation of higher-order harmonics, for example in the nonlinear (strong current) regime and under time-dependent perturbation (irradiation of the electron system by electromagnetic waves). In these cases, nontrivial distributions of the current density and electrochemical potential in the presence of boundaries are expected as well.

Our study reveals an unusual temperature dependence of thermoelectric effects, in particular a suppression of the Nernst voltage by temperature, which cannot be explained either within the diffusive mechanism or within the phonon drag caused by weakly nonequilibrium phonons. The theory we propose describes the effect of temperature in terms of

increasing probability of electron-electron scattering, which is responsible for suppression of higher-order angular harmonics of the electron distribution function. Whereas the general formalism, based on the classical kinetic equation with boundary conditions, is very similar to that used in the description of the magnetoresistance of mesoscopic channels (see [20] and references therein), the thermoelectric problem considered in this paper is essentially different from the magnetoresistance problem. In the latter case, the higher-order angular harmonics appear in the system near the boundaries due to the boundary scattering, while in our case they are created by the phonon-induced excitation in the bulk of the channel. For this reason, a hydrodynamic approach to the problem cannot be applied, and the kinetic equation formalism is necessary for the description of magnetothermoelectric phenomena. A good agreement between experimental and theoretical suppression of the Nernst voltage by temperature is obtained when we use the parameters [in particular, the constant A in Eq. (13)] extracted from a comparison of experimental and theoretical magnetoresistance of narrow channels in mesoscopic Hall bars fabricated from the same 2D layer structures as the H-shaped mesoscopic bars used in our thermoelectric measurements [20].

On the other hand, there is a lack of full qualitative agreement between experiment and theory, which we attribute to a number of simplifying approximations used in the theoretical description of the thermoelectric response. Among them are the neglect of classical memory effects [34], which are not accounted for by the Boltzmann equation but may become important in systems with boundaries in magnetic field; the use of unified scattering lengths l_1 and l_e for all harmonics of the distribution function, which is a crude approximation, especially because of the different sensitivity of even and odd angular harmonics to electron-electron scattering [35]; a simplified device geometry; and a model description of the drag force term in the kinetic equation. In spite of this, we believe that the basic theoretical ideas described in this paper have a potential for further development and can be helpful for a better understanding of electron response in the systems with boundaries and, generally, in inhomogeneous systems of interacting electrons under different types of excitation. We also expect that the results described above will stimulate experimental studies of magnetothermoelectric phenomena in mesoscopic 2D electron systems.

ACKNOWLEDGMENTS

The authors acknowledge financial support of this work by FAPESP and CNPq (Brazilian agencies).

APPENDIX A: PHONON DRAG FORCE

In the classical transport regime, the absorption and stimulated emission of three-dimensional phonons by 2D electrons is described by the phonon drag part of the collision integral:

$$\begin{aligned} \mathcal{J}_{\mathbf{p}}^D = & \frac{2\pi}{\hbar} \sum_{\lambda} \int \frac{d\mathbf{q}}{(2\pi)^2} \int_{-\infty}^{\infty} \frac{dq_z}{2\pi} I_{q_z} C_{\lambda} \mathbf{Q} N_{\lambda} \mathbf{Q} \\ & \times \{ [f_{\mathbf{p}-\hbar\mathbf{q}} - f_{\mathbf{p}}] \delta(\varepsilon_{\mathbf{p}} - \varepsilon_{\mathbf{p}-\hbar\mathbf{q}} - \hbar\omega_{\lambda} \mathbf{Q}) \\ & + [f_{\mathbf{p}+\hbar\mathbf{q}} - f_{\mathbf{p}}] \delta(\varepsilon_{\mathbf{p}} - \varepsilon_{\mathbf{p}+\hbar\mathbf{q}} + \hbar\omega_{\lambda} \mathbf{Q}) \}, \quad (\text{A1}) \end{aligned}$$

where $C_{\lambda\mathbf{Q}}$ is the squared matrix element of electron-phonon interaction in the bulk, $\omega_{\lambda\mathbf{Q}}$ is the phonon frequency, $\mathbf{Q} = (\mathbf{q}, q_z)$ is the phonon wave vector, λ is the phonon mode index (one longitudinal acoustic mode, $\lambda = l$, and two transverse acoustic modes, $\lambda = t_1, t_2$, are considered), and $N_{\lambda\mathbf{Q}}$ is the nonequilibrium part of phonon distribution function. The squared overlap integral $I_{q_z} = |\langle 0 | e^{iq_z z} | 0 \rangle|^2$ depends on the confinement potential defining the ground state of 2D electrons, $|0\rangle$. If $q_z \rightarrow 0$, one has $I_{q_z} = 1$.

To find the effective force acting on electrons due to the drag effect in the linear transport regime, it is sufficient to substitute the equilibrium distribution functions f_ε in Eq. (A1). In the quasielastic approximation, the first and the second square brackets in Eq. (A1) are reduced to $\mp \hbar \omega_{\lambda\mathbf{Q}} (\partial f_\varepsilon / \partial \varepsilon)$, respectively, because small inelastic corrections can be neglected in view of the smallness of phonon energies with respect to the Fermi energy. For the same reason, one may neglect the phonon energy $\hbar \omega_{\lambda\mathbf{Q}}$ in the δ functions in Eq. (A1). The phonon drag collision integral standing in the linearized kinetic equation is then written as $\mathcal{J}_{\varepsilon\varphi}^D \simeq -(\partial f_\varepsilon / \partial \varepsilon) J_{\varepsilon\varphi}^D$, where

$$J_{\varepsilon\varphi}^D \equiv F_{\varepsilon\varphi} v_\varepsilon = \sum_\lambda \int \frac{d\mathbf{q}}{(2\pi)^2} \int_{-\infty}^{\infty} dq_z I_{q_z} C_{\lambda\mathbf{Q}} N_{\lambda\mathbf{Q}} \frac{2m\omega_{\lambda\mathbf{Q}}}{\hbar q} [\delta(\hbar q - 2p_\varepsilon \cos(\varphi - \varphi_q)) - \delta(\hbar q + 2p_\varepsilon \cos(\varphi - \varphi_q))], \quad (\text{A2})$$

$p_\varepsilon = \sqrt{2m\varepsilon}$, and φ_q is the angle of \mathbf{q} .

The use of a standard weakly anisotropic form of $N_{\lambda\mathbf{Q}} \propto \mathbf{Q} \cdot \nabla T$ (see, for example, [3]) reduces the frictional force term $J_{\varepsilon\varphi}^D$ to $e\mathbf{E}_\varepsilon^* \cdot \mathbf{v}$, where $\mathbf{E}_\varepsilon^* \propto \nabla T$ is the effective electric field. To take into account the interaction of electrons with ballistic phonons, another form of $N_{\lambda\mathbf{Q}}$ is required, as described below.

If the ballistic phonons are described as blackbody radiation characterized by the heater temperature T_{ph} , one may write the distribution function as follows:

$$N_{\lambda\mathbf{Q}} = \frac{\mathcal{P}(\zeta, \varphi_q)}{\exp(\hbar\omega_{\lambda\mathbf{Q}}/T_{\text{ph}}) - 1}. \quad (\text{A3})$$

The energy distribution of these phonons is given by Planck's function, while $\mathcal{P}(\zeta, \varphi_q)$ specifies the angular distribution, where ζ is the angle between \mathbf{Q} and z axis. Below we assume a simple case when the flux is homogeneous (independent of coordinate) and unidirectional in the 2D layer plane (like a "phonon beam," since only the phonons that can interact with 2D electrons are relevant), so one can choose the direction of propagation as the x axis: $\zeta \rightarrow \pi/2$ and $\varphi_q \rightarrow 0$. As a result, $\mathcal{P}(\zeta, \varphi_q) = P_0 \delta(\zeta - \pi/2) \delta(\varphi_q)$. This may correspond, for example, to a model of a remote heater, when the distance from the heater to the 2D sample is much larger than the sizes of both the heater and the sample. The proportionality coefficient P_0 can be related to the energy density flux $\phi_{\text{ph}} = \sum_\lambda \int \frac{d\mathbf{Q}}{(2\pi)^3} \hbar \omega_{\lambda\mathbf{Q}} s_\lambda(q_x/Q) N_{\lambda\mathbf{Q}}$, where the isotropic dispersion $\omega_{\lambda\mathbf{Q}} = s_\lambda Q$ is implied:

$$\phi_{\text{ph}} = \frac{\pi P_0 T_{\text{ph}}^4}{120 \hbar^3} \left(\frac{1}{s_l^2} + \frac{2}{s_t^2} \right). \quad (\text{A4})$$

Interaction of electrons with acoustic phonons via the deformation potential gives a contribution to $C_{\lambda\mathbf{Q}}$ equal to

$\delta_{\lambda l} \hbar \mathcal{D}^2 Q / 2\rho_M s_l$, where \mathcal{D} is the deformation potential constant and ρ_M is the material density. The other contribution comes from the interaction via piezoelectric potential and depends on the direction of \mathbf{Q} with respect to crystallographic orientation. Assuming that the z axis coincides with one of the main crystallographic axes, and one of the other main axes is at an angle χ with respect to the x axis, the total contribution is written as

$$C_{\lambda\mathbf{Q}} = \delta_{\lambda l} \frac{\hbar}{2\rho_M s_l Q} \left[\mathcal{D}^2 Q^2 + (eh_{14})^2 \frac{9q_z^2 q^4 \Psi_{\varphi_q}}{2Q^6} \right] + (\delta_{\lambda t_1} + \delta_{\lambda t_2}) \frac{\hbar (eh_{14})^2}{2\rho_M s_l Q} \left[2 \frac{q_z^2 q^2}{Q^4} + \frac{q^4 (q^2 - 8q_z^2) \Psi_{\varphi_q}}{4Q^6} \right], \quad (\text{A5})$$

where h_{14} is the piezoelectric constant and $\Psi_{\varphi_q} = 1 - \cos(4\varphi_q - 4\chi)$ is the orientational form-factor. If phonons are propagating along the 2D plane, $\mathcal{P}(\zeta, \varphi_q) \propto \delta(\zeta - \pi/2)$, so that $q_z = 0$, this general expression simplifies to

$$C_{\lambda\mathbf{Q}} = \delta_{\lambda l} \frac{\hbar \mathcal{D}^2 Q}{2\rho_M s_l} + (\delta_{\lambda t_1} + \delta_{\lambda t_2}) \frac{\hbar (eh_{14})^2 \Psi_{\varphi_q}}{8\rho_M s_l Q}. \quad (\text{A6})$$

Assuming that the heater temperature T_{ph} exceeds the Bloch-Grüneisen temperature so that Planck's function in $N_{\lambda\mathbf{Q}}$ of Eq. (A3) is approximately reduced to $T_{\text{ph}}/\hbar\omega_{\lambda\mathbf{Q}}$, and also assuming that the phonon flux is unidirectional, $\mathcal{P}(\zeta, \varphi_q) = P_0 \delta(\zeta - \pi/2) \delta(\varphi_q)$, one gets the "drag force" $F_{\varepsilon\varphi}$ in Eq. (3) in the following form:

$$F_{\varepsilon\varphi} = \frac{m^2 T_{\text{ph}} P_0}{(2\pi \hbar)^2 \rho_M} \left[\frac{4\mathcal{D}^2 p_\varepsilon}{s_l \hbar^2} \cos^2 \varphi + \frac{(eh_{14})^2 (1 - \cos 4\chi)}{2s_t p_\varepsilon} \right] \times \text{sgn}(\cos \varphi), \quad (\text{A7})$$

and F_φ in Eq. (4) is given by Eq. (A7) with p_ε replaced by the Fermi momentum p_F . For comparison with experiment in Sec. IV, we use the form averaged over the angle χ . If one considers either piezoelectric or deformation potential interaction, F_φ is represented in the simple form of Eq. (8).

APPENDIX B: FUNCTIONS ENTERING EQ. (7)

The formalism leading to Eq. (7) is based on the method of characteristics and is described in more detail in the Appendix to Ref. [20]. Below we present a list of the expressions necessary to obtain the functions entering Eq. (7). These functions have the following form ($n = 0, 1, n' = 0, 1$):

$$\mathcal{K}_{nn'}(y, y') = \int_0^\pi \frac{d\varphi}{2\pi} (2 \cos \varphi)^n (\cos \varphi')^{n'} Q_\varphi^+(y, y') + [\mu_0^n(y) a_{00} + \mu_L^n(y) a_{L0}] \zeta_0^{n'}(y') + [\mu_0^n(y) a_{0L} + \mu_L^n(y) a_{LL}] \zeta_L^{n'}(y'), \quad (\text{B1})$$

$$\mathcal{L}_n(y) = \int_0^\pi \frac{d\varphi}{2\pi} \int_0^L dy' (2 \cos \varphi)^n \cos \varphi' Q_\varphi^+(y, y') + [\mu_0^n(y) a_{00} + \mu_L^n(y) a_{L0}] \int_0^L dy' \zeta_0^1(y') + [\mu_0^n(y) a_{0L} + \mu_L^n(y) a_{LL}] \int_0^L dy' \zeta_L^1(y'), \quad (\text{B2})$$

$$\begin{aligned} \Lambda_n(y) &= \int_0^\pi \frac{d\varphi}{2\pi} \int_0^L dy' (2 \cos \varphi)^n \sum_{s=\pm} F_\varphi^s \mathcal{Q}_\varphi^s(y, y') \\ &+ [\mu_0^n(y)a_{00} + \mu_L^n(y)a_{L0}] \int_0^L dy' \eta_0(y') \\ &+ [\mu_0^n(y)a_{0L} + \mu_L^n(y)a_{LL}] \int_0^L dy' \eta_L(y'). \end{aligned} \quad (\text{B3})$$

where $F_\varphi^\pm = (F_\varphi \pm F_{2\pi-\varphi})/2$. If phonon flux is parallel to the channel, $F_\varphi^- = 0$ and $F_\varphi^+ = F_\varphi$.

Here and below,

$$\varphi' = \arccos[\cos \varphi + (y - y')/R], \quad (\text{B4})$$

$$\begin{aligned} \mathcal{Q}_\varphi^\pm(y, y') &= \{[\theta(\varphi - \varphi') + (1 - d)/d]e^{p(\varphi' - \varphi)} \\ &\pm r_{\varphi_0}^0 e^{p(2\varphi_0 - \varphi - \varphi')}/d + r_{\varphi_L}^L e^{p(\varphi + \varphi' - 2\varphi_L)}/d \\ &\pm [\theta(\varphi' - \varphi) + (1 - d)/d]e^{p(\varphi - \varphi')}\} \frac{1}{\sin \varphi'}, \end{aligned} \quad (\text{B5})$$

where θ is the theta-function and $p = R/l$. The quantities φ_0 , φ_L , and d are functions of $y + R \cos \varphi$:

$$\begin{aligned} \varphi_0 &= \arccos(\min\{1, \cos \varphi + y/R\}), \\ \varphi_L &= \arccos(\max\{-1, \cos \varphi + (y - L)/R\}), \end{aligned} \quad (\text{B6})$$

and

$$d = 1 - r_{\varphi_0}^0 r_{\varphi_L}^L e^{2p(\varphi_0 - \varphi_L)}. \quad (\text{B7})$$

The scalar coefficients in Eqs. (B1)–(B3) are $a_{00} = (\mathcal{N}_L - \alpha_L)/Z$, $a_{L0} = \beta_L/Z$, $a_{0L} = \beta_0/Z$, $a_{LL} = (\mathcal{N}_0 - \alpha_0)/Z$, with $Z = (\mathcal{N}_0 - \alpha_0)(\mathcal{N}_L - \alpha_L) - \beta_0\beta_L$, where \mathcal{N}_0 and \mathcal{N}_L are defined in the main text, while

$$\begin{aligned} \alpha_0 &= \int_0^\pi \frac{d\varphi}{d_0} (1 - r_\varphi^0)^2 r_{\varphi_{L0}}^L \sin \varphi e^{2p(\varphi - \varphi_{L0})}, \\ \alpha_L &= \int_0^\pi \frac{d\varphi}{d_L} (1 - r_\varphi^L)^2 r_{\varphi_{0L}}^0 \sin \varphi e^{2p(\varphi_{0L} - \varphi)}, \\ \beta_0 &= \int_0^\pi \frac{d\varphi}{d_0} (1 - r_\varphi^0)(1 - r_{\varphi_{L0}}^L) \sin \varphi e^{p(\varphi - \varphi_{L0})}, \\ \beta_L &= \int_0^\pi \frac{d\varphi}{d_L} (1 - r_\varphi^L)(1 - r_{\varphi_{0L}}^0) \sin \varphi e^{p(\varphi_{0L} - \varphi)}. \end{aligned} \quad (\text{B8})$$

Here φ_{L0} and d_0 denote φ_L and d at $y = 0$, respectively, while φ_{0L} and d_L denote φ_0 and d at $y = L$.

Finally,

$$\begin{aligned} \mu_0^n(y) &= \int_0^\pi d\varphi (2 \cos \varphi)^n \frac{1 - r_{\varphi_0}^0}{2\pi d} \\ &\times [e^{p(\varphi_0 - \varphi)} + r_{\varphi_L}^L e^{p(\varphi + \varphi_0 - 2\varphi_L)}], \end{aligned} \quad (\text{B9})$$

$$\begin{aligned} \mu_L^n(y) &= \int_0^\pi d\varphi (2 \cos \varphi)^n \frac{1 - r_{\varphi_L}^L}{2\pi d} \\ &\times [r_{\varphi_0}^0 e^{p(2\varphi_0 - \varphi - \varphi_L)} + e^{p(\varphi - \varphi_L)}], \end{aligned} \quad (\text{B10})$$

$$\begin{aligned} \zeta_0^n(y') &= \int_0^\pi d\varphi \left\{ (1 - r_\varphi^0) \frac{\sin \varphi (\cos \varphi')^n}{d \sin \varphi'} \right. \\ &\times \left. \left[e^{p(\varphi - \varphi')} + e^{p(\varphi' - \varphi)} \frac{(1 - d)}{r_\varphi^0} \right] \right\}_{y=0}, \end{aligned} \quad (\text{B11})$$

$$\begin{aligned} \zeta_L^n(y') &= \int_0^\pi d\varphi \left\{ (1 - r_\varphi^L) \frac{\sin \varphi (\cos \varphi')^n}{d \sin \varphi'} \right. \\ &\times \left. \left[e^{p(\varphi' - \varphi)} + e^{p(\varphi - \varphi')} \frac{(1 - d)}{r_\varphi^L} \right] \right\}_{y=L}, \end{aligned} \quad (\text{B12})$$

$$\begin{aligned} \eta_0(y') &= \int_0^\pi d\varphi \left\{ (1 - r_\varphi^0) \frac{\sin \varphi}{d \sin \varphi'} \left[F_{2\pi - \varphi'} e^{p(\varphi - \varphi')} \right. \right. \\ &\left. \left. + F_{\varphi'} e^{p(\varphi' - \varphi)} \frac{(1 - d)}{r_\varphi^0} \right] \right\}_{y=0}, \end{aligned} \quad (\text{B13})$$

$$\begin{aligned} \eta_L(y') &= \int_0^\pi d\varphi \left\{ (1 - r_\varphi^L) \frac{\sin \varphi}{d \sin \varphi'} \left[F_{\varphi'} e^{p(\varphi' - \varphi)} \right. \right. \\ &\left. \left. + F_{2\pi - \varphi'} e^{p(\varphi - \varphi')} \frac{(1 - d)}{r_\varphi^L} \right] \right\}_{y=L}. \end{aligned} \quad (\text{B14})$$

The quantities $\zeta_i^n(y')$ and $\eta_i(y')$ depend on y' through φ' . With the use of Eq. (B4), the integrals over y' in Eqs. (B2) and (B3) can be transformed into integrals over φ' in the interval $\varphi' \in [\varphi_0, \varphi_L]$ and calculated analytically (for fixed φ) if the form of $F_{\varphi'}$ is simple enough. The remaining integrals over φ have to be calculated numerically.

The limiting case of $B = 0$ is equivalent to $R \rightarrow \infty$. It is described by the substitutions

$$\begin{aligned} p(\varphi - \varphi') &= (y - y')/l \sin \varphi, \\ p(\varphi - \varphi_0) &= y/l \sin \varphi, \\ p(\varphi - \varphi_L) &= (y - L)/l \sin \varphi, \\ p(\varphi - \varphi_{0L}) &= p(\varphi_{L0} - \varphi) = L/l \sin \varphi, \end{aligned} \quad (\text{B15})$$

in the exponents of the above expressions and $\theta(\varphi - \varphi') \rightarrow \theta(y - y')$. In all other places, it is sufficient to replace φ_0 and φ_L by φ . In this way, one gets, for example, $d = 1 - r_\varphi^0 r_\varphi^L \lambda_\varphi^2$, where $\lambda_\varphi = \exp(-L/l \sin \varphi)$.

[1] R. Fletcher, *Semicond. Sci. Technol.* **14**, R1 (1999).

[2] R. Fletcher, E. Zaremba, and U. Zeitler, Phonon drag thermopower of low dimensional systems, in *Electron-Phonon Interactions in Low-Dimensional Structures*, edited by L. Challis (Oxford University Press, Oxford, 2003), Chap. 5.

[3] A. Miele, R. Fletcher, E. Zaremba, Y. Feng, C. T. Foxon, and J. J. Harris, *Phys. Rev. B* **58**, 13181 (1998).

[4] D. G. Cantrell and P. N. Butcher, *J. Phys. C* **20**, 1985 (1987); **20**, 1993 (1987).

[5] X. Zianni, P. N. Butcher, and M. J. Kearney, *Phys. Rev. B* **49**, 7520 (1994).

[6] R. Fletcher, J. J. Harris, C. T. Foxon, M. Tsaousidou, and P. N. Butcher, *Phys. Rev. B* **50**, 14991 (1994).

- [7] R. Fletcher, V. M. Pudalov, and S. Cao, *Phys. Rev. B* **57**, 7174 (1998).
- [8] P. N. Butcher and M. Tsaousidou, *Phys. Rev. Lett.* **80**, 1718 (1998).
- [9] B. Tieke, R. Fletcher, J. C. Maan, W. Dobrowolski, A. Mycielski, and A. Wittlin, *Phys. Rev. B* **54**, 10565 (1996).
- [10] O. E. Raichev, *Phys. Rev. B* **91**, 235307 (2015).
- [11] H. Karl, W. Dietsche, A. Fischer, and K. Ploog, *Phys. Rev. Lett.* **61**, 2360 (1988).
- [12] V. I. Fal'ko and S. V. Iordanskii, *J. Phys.: Condens. Matter* **4**, 9201 (1992).
- [13] F. Dietzel, W. Dietsche, and K. Ploog, *Phys. Rev. B* **48**, 4713 (1993).
- [14] W. M. Gancza, C. Jasiukiewicz, A. J. Kent, D. Lehmann, T. Paszkiewicz, K. R. Strickland, and R. E. Strickland, *Semicond. Sci. Technol.* **11**, 1030 (1996).
- [15] E. D. Eidelman and A. Ya. Vul', *J. Phys.: Condens. Matter* **19**, 266210 (2007).
- [16] J. Zhang, S. K. Lyo, R. R. Du, J. A. Simmons, and J. L. Reno, *Phys. Rev. Lett.* **92**, 156802 (2004).
- [17] A. D. Levin, Z. S. Momtaz, G. M. Gusev, O. E. Raichev, and A. K. Bakarov, *Phys. Rev. Lett.* **115**, 206801 (2015).
- [18] I. Mandal and A. Lucas, *Phys. Rev. B* **101**, 045122 (2020), and references therein.
- [19] R. N. Gurzhi, *Sov. Phys. JETP* **44**, 771 (1963).
- [20] O. E. Raichev, G. M. Gusev, A. D. Levin, and A. K. Bakarov, *Phys. Rev. B* **101**, 235314 (2020).
- [21] T. Scaffidi, N. Nandi, B. Schmidt, A. P. Mackenzie, and J. E. Moore, *Phys. Rev. Lett.* **118**, 226601 (2017).
- [22] P. S. Alekseev and M. A. Semina, *Phys. Rev. B* **100**, 125419 (2019).
- [23] T. Holder, R. Queiroz, T. Scaffidi, N. Silberstein, A. Rozen, J. A. Sulpizio, L. Ella, S. Ilani, and A. Stern, *Phys. Rev. B* **100**, 245305 (2019).
- [24] K. Fuchs, *Proc. Cambridge Philos. Soc.* **34**, 100 (1938).
- [25] S. B. Soffer, *J. Appl. Phys.* **38**, 1710 (1967).
- [26] M. J. M. de Jong and L. W. Molenkamp, *Phys. Rev. B* **51**, 13389 (1995).
- [27] B. R. Cyca, R. Fletcher, and M. D'Iorio, *J. Phys.: Condens. Matter* **4**, 4491 (1992).
- [28] See Supplemental Material at <http://link.aps.org/supplemental/10.1103/PhysRevB.102.195301> for details of the experimental setup and measurements.
- [29] A. G. Pogosov, M. V. Budantsev, D. Uzur, A. Nogaret, A. E. Plotnikov, A. K. Bakarov, and A. I. Toropov, *Phys. Rev. B* **66**, 201303(R) (2002).
- [30] S. Maximov, M. Gbordzoe, H. Buhmann, L. W. Molenkamp, and D. Reuter, *Phys. Rev. B* **70**, 121308(R) (2004).
- [31] S. Goswami, C. Siegert, M. Baenninger, M. Pepper, I. Farrer, D. A. Ritchie, and A. Ghosh, *Phys. Rev. Lett.* **103**, 026602 (2009).
- [32] S. Goswami, C. Siegert, M. Pepper, I. Farrer, D. A. Ritchie, and A. Ghosh, *Phys. Rev. B* **83**, 073302 (2011).
- [33] A. D. Levin, G. M. Gusev, E. V. Levinson, Z. D. Kvon, and A. K. Bakarov, *Phys. Rev. B* **97**, 245308 (2018).
- [34] V. V. Cheianov, A. P. Dmitriev, and V. Yu. Kachorovskii, *Phys. Rev. B* **70**, 245307 (2004).
- [35] R. N. Gurzhi, A. N. Kalinenko, and A. I. Kopeliovich, *Phys. Rev. Lett.* **74**, 3872 (1995); *Low Temp. Phys.* **23**, 44 (1997).